

Plasma broadening of autoionizing resonances

A K Pradhan^{1,2,3}

¹ Department of Astronomy, ² Chemical Physics Program, ³ Biophysics Graduate Program, Ohio State University, Columbus, Ohio 43210, USA

September 2022

Abstract. A general formulation is developed to demonstrate that atomic autoionizing (AI) resonances are broadened and shifted significantly due to plasma effects across bound-free continua. The theoretical and computational method presented accounts for broadening mechanisms: electron collisional, ion microfields (Stark), thermal Doppler, core excitations, and free-free transitions. *Extrinsic* plasma broadening redistributes and shifts AI resonance strengths while broadly preserving naturally *intrinsic* asymmetries of resonance profiles. Integrated oscillator strengths are conserved as resonance structures dissolve into continua with increasing electron density. As exemplar, the plasma attenuation of photoionization cross sections computed using the R-matrix method is studied in neon-like Fe XVII in a critical range $N_e = 10^{21-24}$ cc along isotherms $T = 1 - 2 \times 10^6$ K, and its impact on Rosseland Mean opacities. The energy-temperature-density dependent cross sections would elicit and introduce physical features in resonant processes in photoionization, (e + ion) excitation and recombination. The method should be generally applicable to atomic species in high-energy-density (HED) sources such as fusion plasmas and stellar interiors.

1. Introduction

Autoionization (AI) resonances are ubiquitous in atomic reactions. As bound-quasibound-free transitions they manifest themselves in cross sections of atomic processes in a wider variety of shapes, sizes and extent in energy than line formation due to bound-bound transitions. As such, due to generally higher *intrinsic* decay rates relative to radiative rates, it would be expected that AI resonances broaden, smear out, and dissolve into the bound-free continuum far more readily than lines when subjected to *extrinsic* high-energy-density (HED) plasma environments. However, whereas line broadening is an advanced field and is accounted for via elaborate treatments, a theoretical method for AI resonance broadening is not available. Also, although line broadening treatments are precise for hydrogenic and simple atomic systems, several approximations need to be made using fitting formulae, Gaunt factors, etc., for complex atomic systems involving large numbers of transitions for practical applications in laboratory and astrophysical plasmas [1, 2, 3, 4, 5, 6, 7, 8, 9].

Whereas the main broadening mechanisms in AI broadening are physically similar to line broadening, their theoretical and computational treatment is quite different. Superimposed on intrinsic AI broadening in atomic cross sections the extent of resonances owing to extrinsic plasma effects renders much of the line broadening theory inapplicable, particularly for multi-electron systems. The *unbroadened* AI resonances themselves vary by orders of magnitude in width, shapes and heights, and incorporate two types: large features due to photoexcitation-of-core (PEC) below thresholds corresponding to dipole core transitions [10], and infinite Rydberg series of resonances converging on to each excited core level of the (e + ion) system. The generally employed Voigt line profiles obtained by convolution of a Lorentzian function for radiative and collisional broadening, and a Gaussian function for Doppler or thermal broadening, are found to be practically inapplicable for AI broadening. Numerically, the Voigt kernel is ill-conditioned since the collisional-to-Doppler width ratio Γ_c / Γ_d varies over a far wider range for resonances than lines and therefore unconstrained *a priori* [11, 12].

2. Theoretical and computational method

The physical processes for broadening of AI resonances differ from lines qualitatively and quantitatively. However, line broadening processes and formulae may be generalized to develop a theoretical treatment and computational algorithm outlined herein (details to be presented elsewhere). The convolved bound-free photoionization cross section of level i may be written as:

$$\sigma_i(\omega) = \int \tilde{\sigma}(\omega') \phi(\omega', \omega) d\omega', \quad (1)$$

where σ and $\tilde{\sigma}$ are the cross sections with plasma-broadened and unbroadened AI resonance structures, ω is the photon energy (Rydberg atomic units are used throughout), and $\phi(\omega', \omega)$ is the normalized Lorentzian profile factor in terms of the *total* width Γ due to all AI broadening processes included:

$$\phi(\omega', \omega) = \frac{\Gamma(\omega)/\pi}{x^2 + \Gamma^2}, \quad (2)$$

where $x \equiv \omega - \omega'$. The crucial difference with line broadening is that AI resonances in the (e + ion) system correspond to and are due to quantum mechanical interference between discretized continua defined by excited core ion levels in a multitude of channels. The coupled channel (CC) approximation, such as implemented by the R-matrix (RM) method (viz. [1, 4, 5]), accounts for AI resonances in an (e + ion) system with generally asymmetric profiles (unlike line profiles that are usually symmetric). Schematically, CC-RM calculations are as shown in Fig. 1 for an (e + ion) system with bound and continuum levels.

Given N core ion levels corresponding to resonance structures,

$$\sigma(\omega) = \sum_i^N \left[\int \tilde{\sigma}(\omega') \left[\frac{\Gamma_i(\omega)/\pi}{x^2 + \Gamma_i^2(\omega)} \right] d\omega' \right]. \quad (3)$$

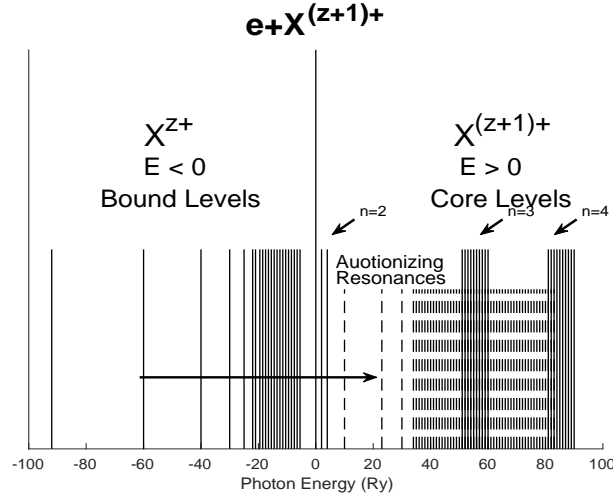


Figure 1. Schematic diagram of coupled channel calculations: photoionization of bound ($e + \text{ion}$) levels into continua of core ion levels (solid lines) $\hbar\omega + X^{z+} \rightarrow e + X^{z+1}$. Rydberg series of AI resonances (dashed lines) converge on to excited core levels at energies $E = E_i - z^2/\nu_i^2$, where ν_i is a continuous variable corresponding to each threshold energy E_i . The schematics approximately refers to Fe XVII cross sections exemplified in Figs. 2 and 3, with 218 $n=2,3,4$ energy levels of Fe XVIII.

With $x \equiv \omega' - \omega$, the summation is over all excited thresholds E_i included in the N -level CC or RM wavefunction expansion, and corresponding to total damping width Γ_i due to all broadening processes. The profile $\phi(\omega', \omega)$ is centered at each continuum energy ω , convolved over the variable ω' and relative to each excited core ion threshold i . In the present formulation we associate the energy to the effective quantum number relative to each threshold $\omega' \rightarrow \nu_i$ to write the total width as:

$$\Gamma_i(\omega, \nu, T, N_e) = \Gamma_c(i, \nu, \nu_c) + \Gamma_s(\nu_i, \nu_s^*) + \Gamma_d(A, \omega) + \Gamma_f(f - f; \nu_i, \nu_i'), \quad (4)$$

pertaining to collisional Γ_c , Stark Γ_s , Doppler Γ_d , and free-free transition Γ_f widths respectively, with additional parameters as defined below. Without loss of generality we assume a Lorentzian profile factor that describes collisional-ion broadening which dominates in HED plasmas. We assume this approximation to be valid since collisional profile wings extend much wider as x^{-2} , compared to the shorter range $\exp(-x^2)$ for thermal Doppler, and $x^{-5/2}$ for Stark broadening (viz. [13]). In Eq. (4) the limits $\mp\infty$ are then replaced by $\mp\Gamma_i/\sqrt{\delta}$; δ is chosen to ensure the Lorentzian profile energy range for accurate normalization. Convolution by evaluation of Eqs. (1-3) is carried out for each energy ω throughout the tabulated mesh of energies used to delineate all AI resonance structures, for each cross section, and each core ion threshold. We employ the following expressions for computations:

$$\Gamma_c(i, \nu) = 5 \left(\frac{\pi}{kT} \right)^{1/2} a_o^3 N_e G(T, z, \nu_i) (\nu_i^4 / z^2), \quad (5)$$

where T , N_e , z , and A are the temperature, electron density, ion charge and atomic weight respectively, and ν_i is the effective quantum number relative to each core ion threshold i : $\omega \equiv E = E_i - \nu_i^2/z^2$ is a continuous variable. The Gaunt factor $G(T, z, \nu_i) = \sqrt{3}/\pi[1/2 + \ln(\nu_i kT/z)]$ ([13, 7, 22, 19]). A factor $(n_x/n_g)^4$ is introduced for Γ_c to allow for doubly excited AI levels with excited core levels n_x relative to the ground configuration n_g (e.g. for Fe XVIII $n_x = 3, 4$ relative to the ground configuration $n_g = 2$). A treatment of the Stark effect for complex systems entails two approaches, one where both electron and ion perturbations are combined (viz. [8, 22]), or separately (viz. [4, 13]) employed herein. Excited Rydberg levels are nearly hydrogenic and ion perturbations are the main broadening effect, though collisional broadening competes significantly increasing with density as well as ν_i^4 (Eq. 5). The total Stark width of a given n -complex is $\approx (3F/z)n^2$, where F is the plasma electric microfield. Assuming the dominant ion perturbers to be protons and density equal to electrons, $N_e = N_p$, we take $F = [(4/3)\pi a_0^3 N_e]^{2/3}$, as employed in the Mihalas-Hummer-Däppen equation-of-state formulation [14].

$$\Gamma_s(\nu_i, \nu_s^*) = [(4/3)\pi a_0^3 N_e]^{2/3} \nu_i^2. \quad (6)$$

In addition, in employing Eq. (6) a Stark ionization parameter $\nu_s^* = 1.2 \times 10^3 N_e^{-2/15} z^{3/5}$ is introduced such that AI resonances may be considered fully dissolved into the continuum for $\nu_i > \nu_s^*$ (analogous to the Inglis-Teller series limit [15, 14]). Calculations are carried out with and without ν_s^* as shown later in Table 1. The Doppler width is:

$$\Gamma_d(A, T, \omega) = 4.2858 \times 10^{-7} \sqrt{(T/A)}, \quad (7)$$

where ω is *not* the usual line center but taken to be each AI resonance energy. The last term Γ_f in Eq. (5) accounts for free-free transitions among autoionizing levels with ν_i, ν'_i such that

$$X_i + e(E_i, \nu_i) \longrightarrow X'_i + e'(E'_i, \nu'_i). \quad (8)$$

The large number of free-free transition probabilities for *ve* energy AI levels $E_i, E'_i > 0$ may be computed using RM or atomic structure codes (viz. [16, 21]).

Whereas Eq.(3) has an analytical solution in terms of $\tan^{-1}(x/\Gamma)/\Gamma$ evaluated at limiting values of $x \rightarrow \mp\Gamma/\sqrt{\delta}$, its evaluation for practical applications entails piecewise integration across multiple energy ranges spanning many excited thresholds and different boundary conditions. For example, the total width Γ is very large at high densities and the Lorentzian profile may be incomplete above the ionization threshold and therefore not properly normalized. We obtain the necessary redward left-wing correction for partial renormalization as

$$\lim_{a \rightarrow -\Gamma/2\sqrt{\delta}} \int_a^{+\Gamma/\sqrt{\delta}} \phi(\omega, \omega') d\omega' = \left[\frac{1}{4} - \frac{\tan^{-1}\left(\frac{a}{\Gamma/2\sqrt{\delta}}\right)}{\pi} \right], \quad (9)$$

where a is the lower energy range up to the ionization threshold, reaching the maximum value $-\Gamma/2\sqrt{\delta}$.

3. Results and discussion

The complexity and magnitude of computations is demonstrated for Fe XVII that is of considerable importance in astrophysical and laboratory plasmas described in a number of previous works ([18] and references therein), owing to its neon-like ground configuration and many excited configurations and n -complexes of levels and transitions. We utilize new results from an extensive Breit-Pauli R-Matrix (BPRM) calculation with 218 fine structure levels dominated by $n = 2, 3, 4$ levels of the core ion Fe XVIII (to be reported elsewhere). The 587 Fe XVII bound levels ($E < 0$) considered are dominated by configurations $1s^2 2s^2 2p^6 ({}^1S_0)$, $1s^2 2s^p 2p^q n\ell$, $[SLJ]$ ($p, q = 0-2$, $n \leq 10$, $\ell \leq 9$, $J \leq 12$). The core Fe XVII levels included in the CC calculation for the $(e + \text{Fe XVIII}) \rightarrow \text{Fe XVII}$ system are: $1s^2 2s^2 2p^5 ({}^2P_{1/2,3/2}^o)$, $1s^2 2s^2 2p^q n\ell$, $[S_i L_i J_i]$ ($p = 4, 5$, $n \leq 4$, $\ell \leq 3$). The Rydberg series of AI resonances correspond to $(S_i L_i J_i) n\ell$, $n \leq 10$, $\ell \leq 9$, with effective quantum number defined as a continuous variable $\nu_i = z/\sqrt{(E_i - E)}$ ($E > 0$), throughout the energy range up to the highest 218th Fe XVIII core level; the $n = 2, 3, 4$ core levels range from $E=0-90.7$ Ry ([17, 18]). The Fe XVII BPRM calculations were carried out resolving the bound-free cross sections at $\sim 40,000$ energies for 454 bound levels with AI resonance structures. Given 217 excited core levels of Fe XVIII, convolution is carried out at each energy or approximately 10^9 times for each (T, N_e) pair.

Fig. 2 displays detailed results for plasma broadened and unbroadened photoionization cross section of one particular excited level $2s^2 2p^5 [{}^2P_{3/2}^o] 4d ({}^1F_3^o)$ (ionization energy = 17.626 Ry) of Fe XVII at three representative densities (note the ~ 10 orders of magnitude variation in resonance heights along the Y-axis). The main feature evident in the figure are as follows. (i) AI resonances begin to show significant broadening and smearing of a multitude of overlapping Rydberg series at $N_e = 10^{21}$ cc. The narrower high- n l resonances dissolve into the continua but stronger low- n l resonance retain their asymmetric shapes with attenuated heights and widths. (ii) As the density increases by one to two order of magnitude, to $N_e = 10^{22-23}$ cc, resonance structures not only broaden but their strengths shift and redistributed over a wide range determined by total width $\Gamma(\omega, \nu_i, T, N_e)$ at each energy $\hbar\omega$ (Eq. 4). (iii) Stark ionization cut-off (Table 1) results in step-wise structures that represent the average due to complete dissolution into continua. (iv) The total AI resonance strengths are conserved, and integrated values generally do not deviate by more than 1-2%. For example, the three cases in Fig. 2: unbroadened structure (black), and broadened without (red) and with Stark cut-off (blue), the integrated numerical values are 59.11, 59.96, 59.94 respectively. This is also an important accuracy check on numerical integration and the computational algorithm, as well as the choice of the parameter δ that determines the energy range of the Lorentizan profile at each T and N_e ; in the present calculations it varies from $\delta = 0.01-0.05$ for $N_e = 10^{21-24}$ cc.

Fig. 3 shows similar results to Fig. 2 for another excited Fe XVII level $2s^2 2p^5 [{}^2P_{3/2}^o] 4d ({}^1F_3^o)$ (ionization energy 17.626 Ry), along a lower temperature 10^6 K isotherm at different intermediate densities. Both Figs. 2 and 3 show a redward shift

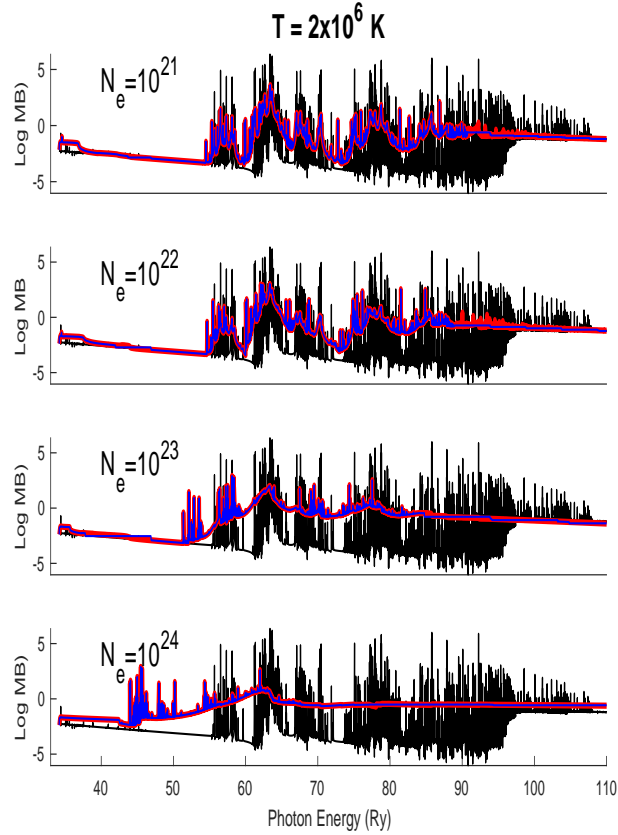


Figure 2. Plasma broadened photoionization cross sections for $\hbar\omega + \text{Fe xvii} \rightarrow e + \text{Fe xviii}$ of the bound level $2s^22p^5[{}^2P_{3/2}^o]3p({}^3D_2)$ (ionization energy 37.707 Ry) along isotherm $T = 2 \times 10^6\text{K}$ and electron densities $N_e = 10^{21,22,23}\text{cc}$: black — unbroadered, red — broadened, blue — broadened with Stark ionization cut-off ν_s^* (Table 1). Rydberg series of AI resonance complexes with $\nu_i \leq 10$ belonging to 217 excited Fe XVIII levels E_i broaden and shift with increasing density, also resulting in continuum raising and threshold lowering.

of low- n resonances and dissolution of high- n resonances. In addition, the background continuum is raised owing to redistribution of resonance strengths, which merge into one across high n and overlapping thresholds. Free-free transitions are not considered in the results in Figs. 2 and 3 but included in the results discussed in Table 1, although it is found to be practically negligible.

Table 1 gives plasma parameters corresponding to Figs. 2 and 3. Their physical significance is demonstrated by a representative sample tabulated temperature $T(\text{K})$ and N_e . The maximum width Γ_{10} corresponding to $\nu_i = 10$ in Eqs. (4-7) is set by the CC-BPRM calculations which delineate unbroadered AI resonance profiles up to $\nu \leq 10$, and employ an averaging procedure up to each threshold $10 < \nu < \infty$ using quantum defect (QD) theory (viz. [20, 4, 5] and references therein). $\Gamma_c(10)$ and $\Gamma_s(10)$ are the maximum collisional and Stark width components. The Doppler width Γ_d is

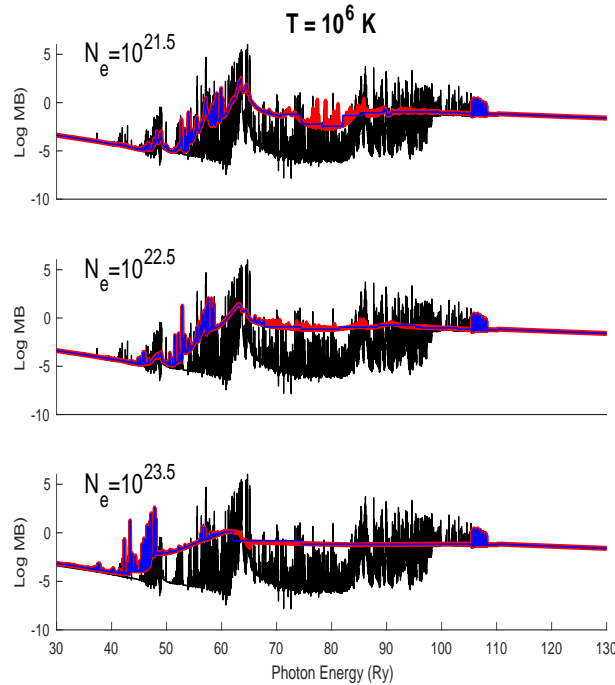


Figure 3. Plasma broadened photoionization cross sections of Fe XVII level $2s^2 2p^5 [^2P_{3/2}^o] 4d(^1F_3^o)$ (ionization energy 17.626 Ry), along isotherm $T = 10^6$ K and electron densities $N_e = 10^{21.5, 22.5, 23.5}$ cc, as in Fig. 2.

much smaller, 1.18×10^{-3} and 1.67×10^{-3} Ry at 10^6 K and 2×10^6 K respectively, validating its inclusion in Eq. (4) in HED plasma sources but possibly not when Γ_d is comparable to Γ_c or Γ_s . The ν_s^* and ν_D are effective quantum numbers corresponding to Stark ionization cut-off and the Debye radius respectively. We obtain $\nu_D = \left[\frac{2}{5} \pi z^2 \lambda_D^2 \right]^{1/4}$, where the Debye length $\lambda_D = (kT/8\pi N_e)^{1/2}$. It is seen in Table 1 that $\nu_D > \nu_s^*$ at the T , N_e considered, justifying neglect of plasma screening effects herein, but which may need to be accounted for at even higher densities.

The aggregate effect of AI broadening for large-scale applications is demonstrated in Table 1 by the ratio R of the Rosseland Mean Opacity using broadened/unbroadened cross sections for 454 Fe XVII levels with AI resonances (other higher bound levels have negligible resonances) [23, 18]. For any atom or ion R is highly dependent on T and N_e ; for Fe XVII R yields up to 58% enhancement due to plasma broadening with increasing N_e along the 2×10^6 K isotherm, but decreasing to 6% along the 10^6 K isotherm. Approximately 70,000 free-free transitions among +ve energy levels are included in the calculation of R , but their contribution has no significant broadening effect since they entail very high-lying levels with negligible level populations. However, different plasma environments with intense radiation fields, or a different equation-of-state than [14] employed here, may lead to more discernible effect due to free-free transitions. AI broadening in a plasma environment affects each level cross section differently, and hence its contribution to opacities or rate equations for atomic processes in general. A

Table 1. Plasma parameters along isotherms in Fig. 2 and 3; ν_D corresponds to Debye radius; R is the ratio of Fe xvii Rosseland Mean Opacity with and without broadening [23]; Γ_{10} is the maximum AI resonance width at $\nu = 10$.

T(K)	$N_e(cc)$	$\Gamma_{10}(Ry)$ $\nu = 10$	$\Gamma_c(10)$	$\Gamma_s(10)$	ν_s^*	ν_D	R
hline 2×10^6	10^{21}	3.42(-1)	8.55(-2)	2.57(-1)	10.4	28.1	1.35
2×10^6	10^{22}	2.05(0)	8.55(-1)	1.19(0)	7.7	15.8	1.43
2×10^6	10^{23}	1.41(1)	8.55(0)	5.53(0)	5.6	8.9	1.55
2×10^6	10^{24}	1.11(2)	8.55(1)	2.57(1)	4.1	5.0	1.58
10^6	$3.1 \times 10^{21.5}$	8.17(-1)	2.71(-1)	5.46(-1)	9.0	17.8	1.47
10^6	$3.1 \times 10^{22.5}$	5.25(0)	2.71(0)	2.53(0)	6.6	10.0	1.13
10^6	$3.1 \times 10^{23.5}$	3.89(0)	2.71(1)	1.18(0)	4.8	5.6	1.06

critical (T, N_e) range can therefore be numerically ascertained where redistribution and shifts of atomic resonance strengths would be significant and cross sections should be modified.

4. Conclusion

The main conclusions are: (I) The method described herein is generally applicable to AI resonances in atomic processes in HED plasmas. (II) The cross sections become energy-temperature-density dependent in a critical range leading to broadening, shifting, and dissolving into continua. (III) Among the approximations necessary to generalize the formalism is the assumption that thermal Doppler widths are small compared to collisional and Stark widths as herein, but given the intrinsic asymmetries of AI resonances it may not lead to significant inaccuracies (although that needs to be verified in future works). (IV) The treatment of Stark broadening and ionization cut-off is *ad hoc*, albeit based on the equation-of-state formulation [14] and consistent with previous works [4]. (V) Since it is negligibly small, the free-free contribution is included post-facto in the computation of the ratio R in Table 1 and not in the cross sections and results shown in Figs. 2 and 3, but may be important in special HED environments with intense radiation and should then be incorporated in the main calculations of total AI width (Eq. 4). (VI) The predicted redward shift of AI resonances as the plasma density increases should be experimentally verifiable. (VII) Redistribution of AI resonance strengths should particularly manifest itself in rate coefficients for (e + ion) excitation and recombination in plasma models and simulations, and for photoabsorption in opacity calculations, using temperature-dependent Maxwellian, Planck, or other particle distribution functions. (VIII) The treatment of individual contributions to AI broadening may be improved, and the theoretical formulation outlined here is predicated on the assumption that

external plasma effects are perturbations subsumed by and overlying the intrinsic autoionization effect. (IX) The computational formalism is designed to be amenable for practical applications and the computational algorithm and a general-purpose program AUTOBRO are optimized for large-scale computations of AI broadened atomic cross sections in HED plasma models. The CPU time required depends mainly on the density which determines the total width Γ ; for example, in the reported calculations for Fe XVII at $T=2 \times 10^6$ K it is few minutes for $N_e = 10^{21}$ cc and ~ 3 hours for $N_e = 10^{24}$ cc.

Acknowledgements

I would like to thank Sultana Nahar for Fe XVII atomic data and discussions.

References

- [1] Burke P G 2011 *R-Matrix Theory of Atomic Collisions*, Springer
- [2] Drake R P 2006 *High Energy Density Physics*, Springer
- [3] Hubeny Ivan and Mihalas Dimitri (2015) *Theory of Stellar Atmospheres*, Princeton University Press
- [4] The Opacity Project Team, 1995 *The Opacity Project*, Institute of Physics Publishing, Vol 1
- [5] Pradhan A K and Nahar S N 2011 *Atomic Astrophysics and Spectroscopy* Cambridge University Press
- [6] Peach G 1981 *Advances in Physics* 30 367
- [7] Dimitrijevic M S and Konjevic N 1981 *Astron. Astrophys.* 102 93
- [8] Dimitrijevic M S and Konjevic N 1987 *Astron. Astrophys.* 172 345
- [9] Konjevic N 1999 *Phys. Repts.* 316 339
- [10] Yu Y and Seaton M J *J. Phys. B* 20 6409
- [11] Hummer D 1965 *Mon. Not. R. astr. Soc.* 70 1
- [12] Several formulations were employed to implement a Voigt profile but were numerically unstable owing to $\Gamma_c \gg \Gamma_d$.
- [13] Seaton M J 1990 *J. Phys. B* 23 3255; see also other papers in [4]
- [14] Mihalas D, Hummer D G and Däppen W 1988 *Astrophys. J.* 331, 815
- [15] Inglis D R and Teller E 1939 *Astrophys. J.* 90 439
- [16] Seaton M J 2000 *J. Phys. B* 33 2677
- [17] Nahar S N, Pradhan A K, Chen G.-X and Eissner W 2011 *Phys. Rev. A* , 83, 053417
- [18] Nahar S N and Pradhan A K 2016 *Phys. Rev. Lett.* 116 235003; Ibid. *Phys. Rev. Lett.* , 117, 249502
- [19] The Gaunt factor $G(T, z, \nu_i)$ depends on T and z, and differs from the similar factor $G(z) = (8\pi/3)\sqrt{3}\bar{g}$, and approaches the fitting formula $G(z)=6.3-5.9/(1+z)$ as $\nu_i \rightarrow 10$ used in [13, 4].
- [20] The QD regions $10 < \nu_i < \infty$ are generally small and overlapping for closely spaced excited core levels, as herein.
- [21] Eissner W, Jones M and Nussbaumer H 1974 *Comput. Phys. Commun.* 8 270
- [22] Xiang W, Zeng J, Fu Y and Gao C 2012 *J. Mod. Phys.*, 3, 1670
- [23] We eschew a discussion of opacities *per se*, as they also depend on accuracy and completeness of atomic data, equation-of-state of the plasma source and other quantities, and focus on AI resonance broadening in atomic processes.